nature portfolio

https://doi.org/10.1038/s41586-022-04512-8

Supplementary information

Observation of a linked-loop quantum state in a topological magnet

In the format provided by the authors and unedited

Supplementary information for: Observation of a linked loop quantum state in a topological magnet

Ilya Belopolski*, Guoqing Chang*, Tyler A. Cochran*, Zi-Jia Cheng*, Xian P. Yang, Cole Hugelmeyer, Kaustuv Manna, Jia-Xin Yin, Guangming Cheng, Daniel Multer, Maksim Litskevich, Nana Shumiya, Songtian S. Zhang, Chandra Shekhar, Niels B. M. Schröter, Alla Chikina, Craig Polley, Balasubramanian Thiagarajan, Mats Leandersson, Johan Adell, Shin-Ming Huang, Nan Yao, Vladimir N. Strocov, Claudia Felser, and M. Zahid Hasan

Contents

1. SOFT X-RAY ARPES SYSTEMATICS

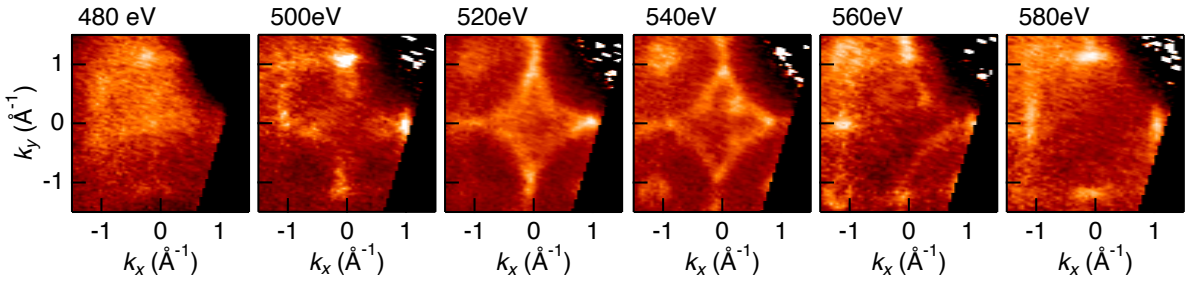

FIG. S1: **SX-ARPES systematics.** Fermi surfaces acquired by SX-ARPES at several photon energies in the vicinity of X_1. The Weyl loop vanishes as k_z shifts away from X_1, at ~ 540 eV.

The Weyl loop around X_1 is restricted to a small range of k_z (Fig. S1). The clearest loop-shaped contour is observed at ~ 540 eV, close to X_1 as pinpointed in our photon energy dependences. Moving away from X_1, we observe some perturbation of the Weyl loop contour, for example at 520 eV. However, the loop rapidly vanishes as we move further away in k_z. Beyond ± 40 eV we find that the loop contributes little spectral weight. This sets a bound of $\delta k_z \sim \pm 0.25 \text{Å}^{-1}$ on the k_z extent of the X_1 loop. Given the convolution with the intrinsic k_z broadening of the SX-ARPES measurement, we can estimate the anisotropy of the Weyl loop Fermi sheets to be $\alpha \sim \delta k_{||}/\delta k_z \sim 0.8 \text{Å}^{-1}/0.2 \text{Å}^{-1} \sim 4$. The highly anisotropic character of the Fermi sheet further supports the presence of Weyl loops confined to the momentum-space mirror planes, which together form an exotic linked Weyl loop structure.

2. VACUUM ULTRAVIOLET ARPES SYSTEMATICS

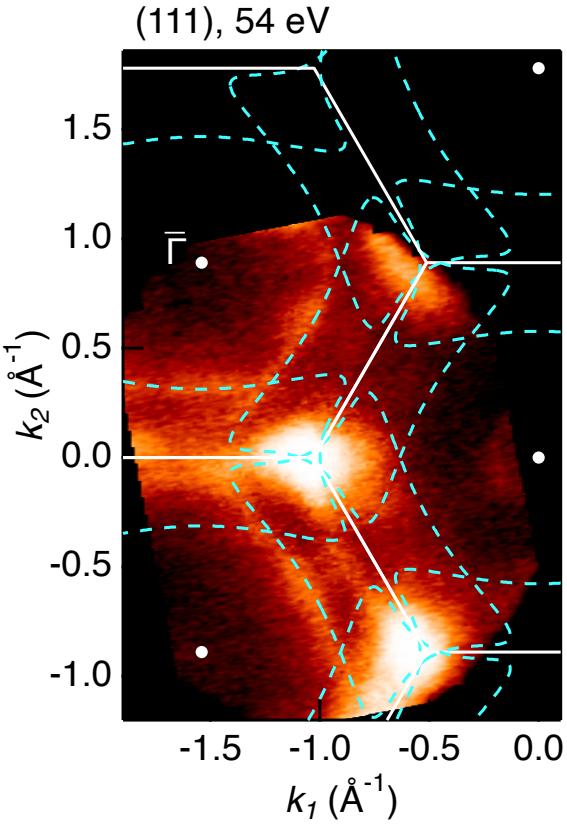

FIG. S2: **Linked Weyl loops in VUV-ARPES.** Fermi surfaces acquired at (**a**), $h\nu = 54$ eV and (**b**), 63 eV, with the Weyl loop trajectory extracted from SX-ARPES superimposed (cyan dashed lines). The Weyl loop observed by SX-ARPES on (001) matches well that observed by VUV-ARPES on (111), allowing us to pinpoint the bulk states in our VUV spectra. The large overlap of the Weyl loops again demonstrates a bulk linked loop structure.

To more carefully compare our SX- and VUV-ARPES results, we consider our Weyl loop trajectory obtained from our systematic SX-ARPES measurements (main text, Fig. 2c) and project it on (111). We then superimpose the projected Weyl loop on a (111) Fermi surface acquired by VUV-ARPES, at $h\nu = 54$ eV (Fig. S2). We observe clear signatures of large Weyl loops, which exhibit excellent quantitative agreement with the projected Weyl loop trajectory. Moreover, we clearly observe that the Weyl loop contours exhibit large overlap on our (111) Fermi surface. Given the oblique orientation of (111) relative to the (100), (010) and (001) mirror planes hosting the Weyl loops, the observation of clear overlapping

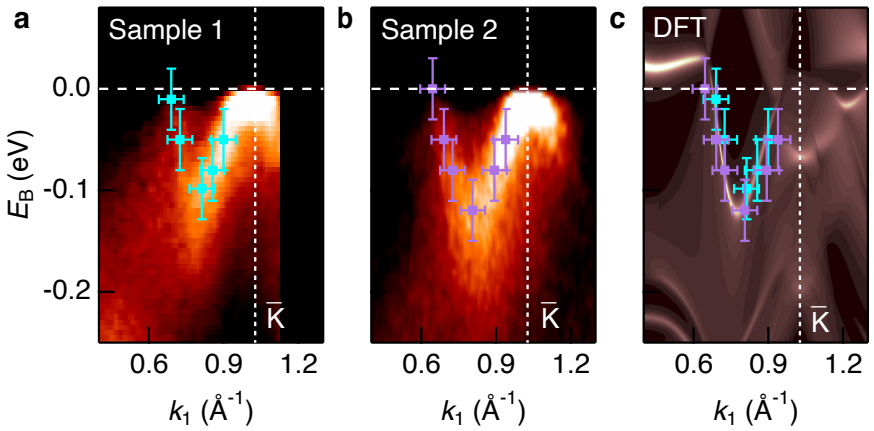

FIG. S3: **Seifert boundary mode.** (**a**), (**b**), ARPES energy-momentum cut through the Seifert boundary modes for two sample cleaves, acquired at $h\nu = 63$ eV, with momentum axis fixed by alignment to the Weyl loops (see Fig. S2). (**c**), Analogous *ab initio* calculation, with ARPES dispersion superimposed (cyan and purple markers). The ARPES and *ab initio* results show good agreement, providing evidence for Seifert boundary modes on the (111) surface of Co_2MnGa.

Weyl loops on (111) provides an independent demonstration of a linked loop quantum state.

We perform additional VUV-ARPES measurements on a second Co_2MnGa sample, which clearly reproduce the surface state of interest. For both samples, we observed quantitative agreement in the dispersions between the VUV-ARPES and surface *ab initio* calculations (Fig. S3). Our new VUV-ARPES measurements on an additional sample; quantitative comparison of the Weyl loop between SX-ARPES and VUV-ARPES; and the quantitative agreement with surface *ab initio* calculations all suggest the observation of Seifert boundary modes arising from the linked loop quantum state. For completeness, we include the momentum-space slices captured our VUV-ARPES Fermi surfaces acquired at $h\nu = 54$ eV and 63 eV (Fig. S4).

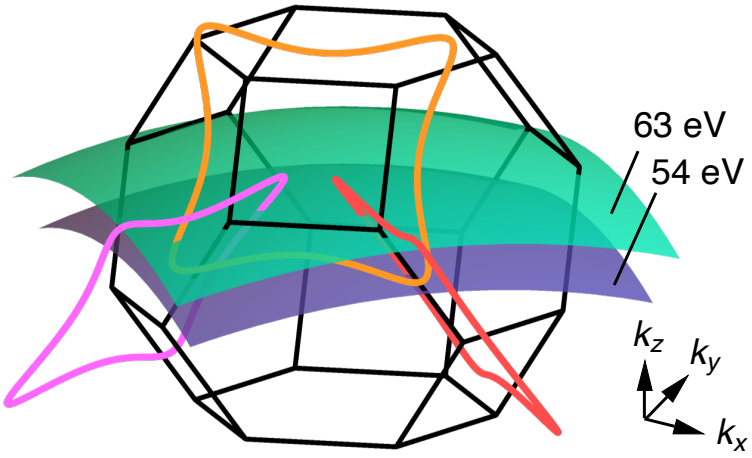

FIG. S4: **Fermi surfaces measured by VUV-ARPES on the** (111) **cleaving plane.** The Brillouin zone corresponds to $\Gamma_{(222)}$ in the conventional reciprocal basis.

3. *AB INITIO* SYSTEMATICS

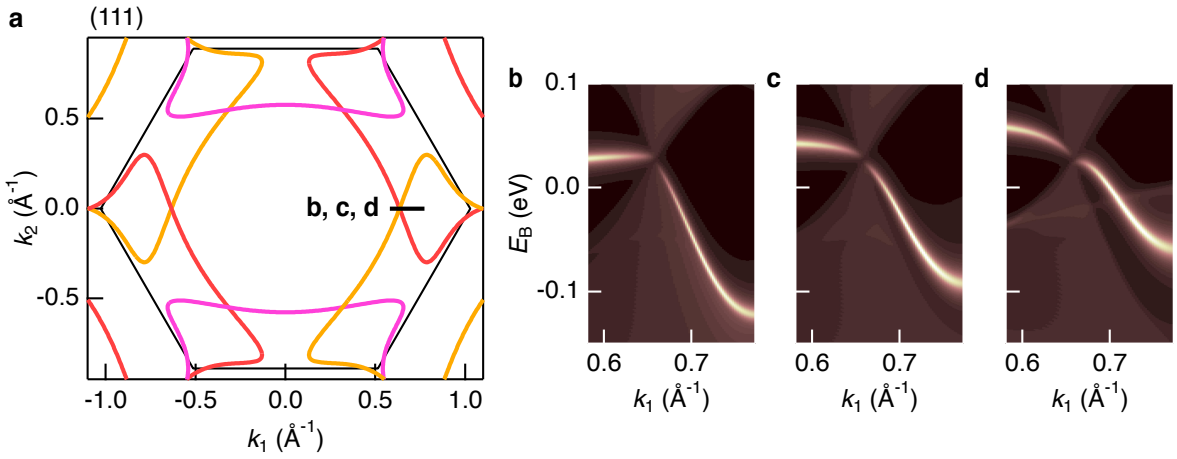

FIG. S5: **Linked Weyl loop Fermi surface.** (**b**), Zoomed-in *ab initio* calculation of the surface states through the Weyl loop 'linking point' on (111), path indicated in (**a**). (**c**), (**d**), Same as (a), but with modified surface chemical potential. The Seifert boundary modes continue to be pinned to the touching point, again demonstrating their topological nature.

The observed surface state is topological and is protected by a quantized winding number. We can theoretically demonstrate that it is topological by examining its behavior under modified surface potential in *ab initio* calculation (Fig. S5). Under such a perturbation, we find that the surface state remains robustly pinned to the linked Weyl loops, showing that it is a Seifert boundary mode and not a topologically-trivial surface resonance.

4. ANALYSIS OF THE LINKING NUMBER

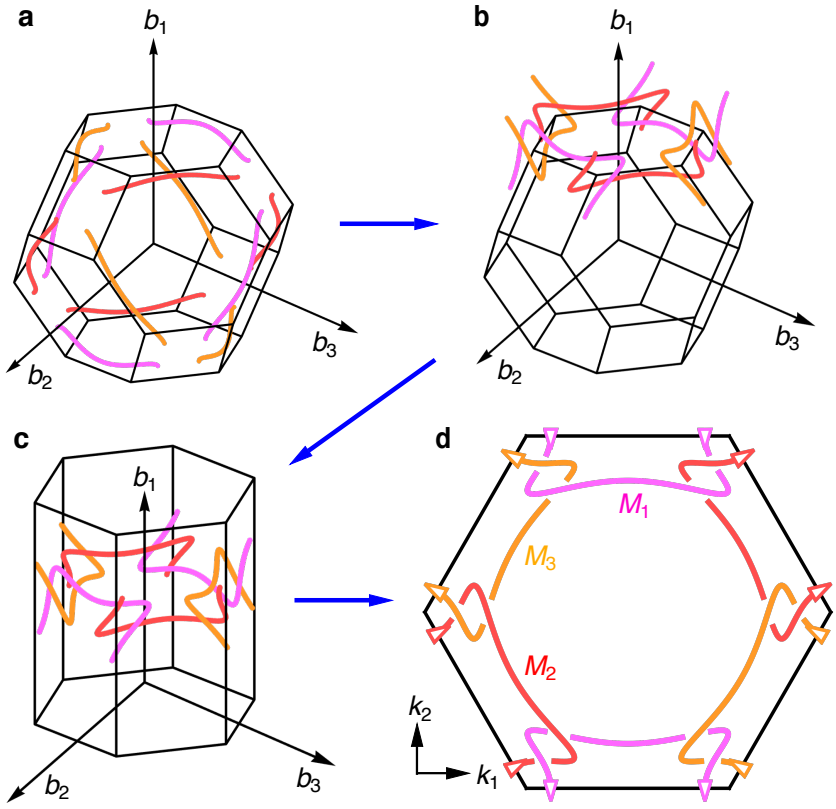

FIG. S6: **Analysis of the linking number.** (**a**), Single copy of the linked node loops, plotted in the first bulk Brillouin zone. (**b**), Again a single copy of the linked node loops, but plotted around a hexagonal face of the Brillouin zone to make the linking more evident. (**c**), The same single copy as in (b), plotted in a non-standard reciprocal primitive unit cell. The chosen primitive cell is a cylindrical prism with the same volume as the bulk Brillouin zone, but which naturally displays the linking for a single copy of the loops and which can be directly projected in the (111), or b_1 direction. (**d**), Link diagram in the (111) surface Brillouin zone following projection, clearly exhibiting linking number $\nu = 2$ between each pair of loops (main text Fig. 4e).

It is important to consider **all loops in a single Brillouin zone** (a reduced zone scheme). Considering fewer loops by ignoring physically-distinct link components does not correctly characterize the linking number. On the other hand, considering the whole of momentum space (an extended zone scheme) introduces redundant copies of the electronic states and is also incorrect. While it may be useful to plot several extra copies of the loops

in order to visualize the link structure, this redundancy must be taken into account when interpreting the linking number. For example, although 6 loops are plotted in Fig. 4b, loops of the same color refer to redundant copies of the same physical states. In total, there are three distinct loops, one of each color. Linking between exactly these three distinct loops determines the linking number.

Considering a single copy of physically-distinct states is typical in condensed matter physics. For example, the density of states of a band structure requires an **integral over a single Brillouin zone**, so that each one-electron level is counted exactly once [Eq. 8.57, Ashcroft & Mermin (1967)],

$$g(\varepsilon) = \int_{\mathrm{BZ}} \frac{d^3k}{4\pi^3} \delta\big(\varepsilon - \bar{\varepsilon}(k)\big) \qquad \text{[integral over one Brillouin zone]}$$

Similarly, a calculation of a Chern number also requires an **integral over a single two-dimensional Brillouin zone** [Eq. 4.4.6, Xiao-Gang Wen (2004)],

$$\sigma_{xy} = \frac{e^2}{h} \frac{1}{2\pi} \int_{\mathrm{BZ}} d^2k \Omega_z(k) \qquad \text{[integral over one Brillouin zone]}$$

In the present case, **it is necessary and sufficient to consider all Weyl loops associated with physically-distinct electronic states.** To further clarify this point, in our revised Supplementary Information we plot a single copy of the Weyl loops in a way which highlights the linking (Fig. S6a,b). Equivalently, we can partition extended momentum space with a non-standard reciprocal primitive unit cell (Fig. S6c). Although it is not the Brillouin zone, this alternative primitive cell has the same volume as the Brillouin zone and contains one copy of the electronic states. This choice of primitive cell naturally pulls out a single set of three loops in a way that manifests the linking structure. This primitive cell further lends itself to projection along (111) or b_1. We can then project the links into the (111) surface Brillouin zone, while preserving the out-of-plane information using an over/under notation. This procedure yields our link diagram and clearly demonstrates linking number $(2, 2, 2)$ for the Co_2MnGa node loops (Fig. S6d, main text Fig. 4e).

5. TOPOLOGY & LINKED LOOP QUANTUM STATES

Knots and links are one of the oldest human technologies; they appear as powerful artistic and religious symbols across human cultures; and in the modern era they have been objects of profound scientific and mathematical interest [J. C. Turner, P. van de Griend, *History and Science of Knots* (1996); C. C. Adams, *The Knot Book* (1994)]. Our discovery of a highly non-trivial quantum linked structure in Co_2MnGa represents an important contribution to this tradition. We elaborate on the significance of our work,

1. **Topology can drive new subfields of science:** Discoveries of new manifestations of topology often open rich new research directions.

   (a) *Organic chemistry:* Breakthroughs in template-directed synthesis of **linked polymer macrocycles** in the early 1980s opened the study of linked catenanes and rotaxanes [J. P. Sauvage, C. Dietrich-Buchecker, *Molecular Catenanes, Rotaxanes and Knots* (1999)], leading to the development of link-based molecular switches, molecular rotary motors and high-specificity electrochemical sensors. Linked organic polymers have come to represent a **triumph of synthetic supramolecular chemistry** [*Ang. Chemie*, **54**, 6110 (2015)].

   (b) *Quantum mechanics:* The discovery that the **Jones polynomial** of knot theory could be associated with vacuum expectation values of Wilson loops in Chern-Simons theory catalyzed the development of **topological quantum field theory** [E. Witten, *Comm. Math. Phys.* **121**, 351 (1989); L. H. Kauffman, R. A. Baadhio, *Quantum Topology* (1993)]. This then contributed to particle physics via the Khovanov homology; deepened our understanding of the electric-magnetic duality, magnetic monopoles and fractional electronic charges; and contributed to the supersymmetric theory of stochastic dynamics [T. Ohtsuki, *Quantum Invariants* (2001)].

   (c) *Condensed matter physics, order parameters:* Windings of order parameters in real space are a unifying theme of condensed matter, encompassing disclinations in liquid crystals; vortices in superconductors and superfluid ^{4}He; and magnetic skyrmions, whose invariants are proposed as the basis for next-generation computing memory and logic.

(d) *Condensed matter physics, band topology:* Momentum-space wavefunction winding is associated with emergent Dirac fermions in two- and three-dimensional topological insulators; Weyl fermions in topological semimetals; and the quantum Hall effect, which sets the prevailing von Klitzing standard of electrical resistance.

Our results provide a new and qualitatively different example of topology in nature: the linking of Weyl loops in electronic structure. The historical importance of earlier topological phenomena suggests that linked node loops are also likely to become a fruitful topic of research.

2. **Seifert boundary modes:** There has been intense interest in observing linked loop states with Seifert boundary modes throughout physics, not only in electronic structures, but also in optics experiments, electric circuits, mechanical systems and cold-atom platforms [*Rev. Mod. Phys.* **93**, 015005]. For the first time, we experimentally demonstrate this unconventional linked topological structure.

3. **Quantized magneto-electric effect:** The axion θ term may give rise to a topological magneto-electric effect in electronic structures hosting linked node loops [*Phys. Rev. B* **96**, 081114(R) (2017), *Phys. Rev. B* **95**, 094512 (2017), *Phys. Rev. Lett.* **119**, 147001 (2017)]. To achieve this effect in Co_2MnGa, we expect that it is first necessary to gap the Weyl loops by breaking mirror symmetry. This could potentially be achieved in thin film samples of Co_2MnGa via an asymmetric substrate-induced lattice strain. Fermi level tuning or perturbation of the electronic structure may then be needed to place the Fermi level in the Weyl loop gap, possibly achieved by engineering the material's magnetic properties via the film substrate, temperature, carrier doping or chemical substitution. Transport or optics experiments may then detect quantized axion electrodynamics, as investigated in topological insulators [*Science* **354**, 1124 (2016)]. In the present case the axion response is expected to be quantized not to the topological insulator $\mathbb{Z}_2$ invariant, but instead to the Weyl loop linking number.

4. **Direct photoemission observation:** Complex magnetic loop node structures have recently attracted considerable interest but **even state-of-the-art analyses have relied on indirect probes** such as de Haas-van Alphen oscillations of topological protectorates in MnSi [*Nature* **594**, 374 (2021)] and the giant anomalous Nernst effect

arising from a Weyl loop network in Fe_3Ga [*Nature* **581**, 53 (2020)]. We provide the first photoemission tomography of a linked loop quantum state, directly measure its linking number, establish a new bridge between physics and knot theory, and observe signatures of a Seifert bulk-boundary correspondence.

5. **Large class of candidate materials:** Dirac loops, Weyl loops and other classes of loop nodes are ubiquitous in crystals. In our present case, the linked loop phase is driven by a combination of mirror symmetry and ferromagnetism. We note that 160 of the 230 space groups contain a mirror or glide symmetry and there are several thousand known ferromagnets, suggesting that more **linked Weyl loop phases await discovery**. Other classes of loop nodes, such as Dirac loops protected by a combination of inversion and time-reversal symmetry, further broaden the list of candidate materials. Future materials discoveries of linked node loop states will likely provide a **rich materials playground for exploring link-quantized magneto-electric effects**, other exotic response and device applications.

6. **Non-Abelian braiding:** Nodal loops can be characterized by non-Abelian topological charges [*Science* **365**, 1273 (2019)], which may allow braiding operations [*Nat. Phys.* **16**, 1137 (2020)]. These results suggest that **magnetic control of the linking number** in a loop node quantum phase, such as the one we discover in Co_2MnGa, may allow a novel form of topological computation.